Robust Photoplethysmographic (PPG) Based Biometric Authentication for Wireless Body Area Networks and m-Health Applications

Conference Paper · March 2016

DOI: 10.1109/NCC.2016.7561152

CITATIONS
14

READS
626

2 authors:

Tilendra Choudhary
Indian Institute of Technology Guwahati
21 PUBLICATIONS **101** CITATIONS

SEE PROFILE

M. Sabarimalai Manikandan
Indian Institute of Technology Bhubaneswar
71 PUBLICATIONS **1,261** CITATIONS

SEE PROFILE

Robust Photoplethysmographic (PPG) Based Biometric Authentication for Wireless Body Area Networks and m-Health Applications

Tilendra Choudhary
Department of Electronics and Electrical Engineering
Indian Institute of Technology Guwahati
Assam-781039. Email:tilendra@iitg.ernet.in

M. Sabarimalai Manikandan
School of Electrical Sciences
Indian Institute of Technology Bhubaneswar
Odisha-751013. Email:msm@iitbbs.ac.in

***Abstract*—In this paper, we present noise-robust photoplethysmographic (PPG) based biometric authentication method for wireless body area networks and m-health applications. The method consists of four steps: (i) preprocessing of PPG signals, (ii) systolic peak detection, (iii) ensemble averaged pulsatile waveform extraction and (iv) pulsatile waveform similarity matching using a normalized cross correlation (NCC) measure. The performance of the proposed method is tested and validated using different types of PPG signals taken from the standard PPG databases. For predefined threshold of 0.997, the NCC-based PPG biometric method achieves an average false rejection rate (FRR) of 0.32 and false acceptance rate (FAR) of 0.32. Performance evaluation results show that the proposed method achieves consistent authentication results as compared to the other methods under different kinds of artifacts and noise.**

I. Introduction

Photoplethysmography (PPG) is a simple non-invasive and low-cost optical technique that can be used to detect blood volume changes in the microvascular bed of tissue. The PPG signal has been used in a wide range of commercially available medical devices for measuring oxygen saturation, blood pressure and cardiac output, assessing autonomic function and also detecting peripheral vascular disease. In recent years, PPG signal is an emerging biometric identifier for human authentication because of the following advantages: universality, uniqueness, robustness to spoofing attacks, intrinsic aliveness detection, adaptive authentication by updating enrolled template with new physiological feature that evolves with time, ease of physiological recording, ease of feature extraction by exploiting the structural patterns of the physiological signal, low-cost signal acquisition, and continuous availability of physiological signals on wearable body area networks (WBAN), home healthcare and m-health monitoring applications [1]-[5]. The feasibility of beat-by-beat patterns and morphological features of PPG signals for biometric authentication is well studied in the previously published works [6]-[8]. Fig. 1 demonstrates the inter-beat correlation between PPG beat patterns of PPG signals for two different subjects. It can be observed that there is a highly significant correlation among the pulsatile cycles of the PPG signal.

978-1-5090-2361-5/16/$31.00

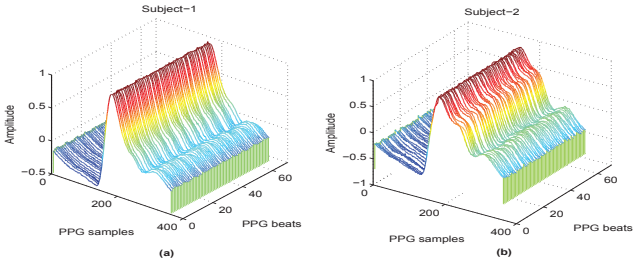

Fig. 1. Illustrates beat-to-beat correlation of PPG signals taken from two different subjects.

Therefore, the inter-pulsatile waveform correlation is exploited in most physiological signal based unimodal and multimodal biometric systems. In the next subsection, we briefly describe the signal processing and pattern recognition techniques used in the existing PPG-based biometric methods.

A. Existing PPG Biometric Methods

Many PPG-based biometric methods have been developed based on the digital filters, beat correlation [6], Fourier analysis and semi discrete decomposition, and Euclidean distance [7], linear discriminant analysis, nearest neighbor classification [8], local maxima/minma and inflection points and time intervals [9], Hamming distance measure [10], fiducial features and discriminant function [11], fuzzy-based decision-making [12], kernel principal component analysis (KPCA) and Mahalanobis distance measure [13], multilayer perceptrons (MLPs), time domain features and k-NN based classification [15].

Many PPG-based biometric methods have been developed based on the pulsatile waveform patterns and/or the local features of the pulsatile waveforms of the PPG signal and the similarity matching or classifiers [6]-[15]. In [6], Bonissi *et al.* presented PPG biometrics based on the third order high pass Butterworth filtering for baseline normalization, peak detection using a modified Pan-Tompkins algorithm, heartbeat averaging and template matching. The method achieves minimum EER of 9%. In [7], Salanke *et al.* presented human identification based on the noise removal using Fourier series analysis,

feature extraction and selection using semi discrete decomposition and Euclidean distance. Spachos *et al.* proposed a PPG biometric identification based on the peak detection, PPG cycle segmentation, normalization, time domain scaling, linear discriminant analysis, nearest neighbor classification. The method achieves an EER of 25% for the test signals of 29 subjects [8]. In [9], Yao *et al.* proposed PPG-based biometric method including the following steps: noise removal using Chebyshev low pass filter, polynomial curve fitting, finding numbers of maxima/minima points and inflection points, and their time intervals from first and second derivatives and correlation. In [11], PPG biometric method based on discriminant function with four feature parameters extracted from PPG signals including, the number of peaks on each pulse, the upward slope of pulse, the downward slope, the time interval between foot and the first peak point. The method achieves a correct verification rate of up to 94%. In [12], Gu and Zhang proposed a PPG authentication using fuzzy-based decision-making with four distinctive features. In [13], Salanke *et al.* proposed an intrinsic PPG biometric method for identifying individual that based on the peak detection and segmentation, feature extraction using kernel principal component analysis (KPCA) and Mahalanobis distance measure. In [14], pattern recognition based on multilayer perceptrons (MLPs) which are employed to learn patterns in time segments around onset and peak points on PPG signal. The method achieves a classification accuracy 98.1%. Kavsaoglu *et al.* presented PPG biometric recognition based on the following stages: pre-processing using FIR filters, time domain features extraction from differentiation stage, distance based feature ranking stage, k-NN based classification [15]. The method achieves 94.44% identification accuracy.

Based on the feature extraction process, the existing PPG based biometric authentication methods can be grouped into four major categories: direct waveform-based methods, pulsatile waveform correlation-based methods, FP (fiducial points)-based methods, and hybrid methods combining the pulsatile waveform correlation and local features of the pulsatile waveform. The pulsatile waveform and fiducial points based methods generally include the steps of: noise removal, peak detection and pulsatile waveform segmentation, feature extraction, and classification using similarity measure or machine learning classifiers. The false rejection rate (FRR) and false acceptance rate (FAR) of most pulsatile waveform-based and FP-based PPG biometric authentication methods highly depends on accurate extraction of pulsatile waveforms (or pulsatile cycles) and reliable measurement of morphological features of the PPG beats under different kinds of artifacts and noise. The presence of motion artifacts in PPG signals is one of the major obstacles in the accurate and reliable measurement of pulsatile waveform features (including, $\mathrm{SP_{amp}}$, $\mathrm{F_{amp}}$, $\mathrm{DP_{amp}}$, $\mathrm{DN_{amp}}$, pulse width (PW), peak-peak interval ($\mathrm{PP_{int}}$), pulse interval, pulse area, inflection point area ratio (IPA), crest time (CT), reflection index (RI), and augmentation index) under varying morphological patterns of pulsatile waveforms and noise conditions. However, a very little attention is paid in developing robust, low-complexity and automatic PPG-based biometric authentication method that has great potential in body area sensor networks and mobile healthcare systems.

In this paper, we attempt to develop a noise-robust pulsatile waveform recognition method in improving accuracy of biometric authentication system under time-varying shapes of the pulsatile waveforms and various kinds of noise. The proposed PPG biometric method consists of four major stages: preprocessing, systolic peak detection, ensemble averaged pulsatile waveform extraction, and similarity matching using a normalized cross correlation metric. The rest of the paper is organized as follows. In Section II, we present the proposed PPG-based biometric method. In Section III, we evaluate the performance of the proposed method using clean and noisy PPG signals. Finally, conclusions are drawn in Section IV.

II. Proposed PPG based Biometric Authentication

In this paper, we present noise-robust PPG biometric method using pulsatile waveform correlation. The method consists of four steps: (i) preprocessing of PPG signals, (ii) detection of systolic peaks in the processed PPG signal, (iii) ensemble averaged pulsatile waveform extraction and similarity matching using normalized cross correlation (NCC) measure.

A. Preprocessing

The PPG signals are often corrupted by various noises including baseline wanders, power-line interference and instrumentation noises. To suppress noises and artifacts, many noise filtering techniques including derivatives, digital filters, wavelet transform, empirical mode decomposition, adaptive filters and filter banks were used at the processing stage. The signal decomposition approach showed better noise reduction performance compared to the time-domain and frequency domain filtering approaches but at the expense of higher computational load. In this work, we design a preprocessing step that uses a Gaussian derivative filter (GDF) to remove baseline wanders and eliminates high-frequency noises. The length and spread of the Gaussian derivative kernel is determined empirically in such that it can simultaneously preserve the shapes of pulsatile waveforms and suppress the baseline wanders and high-frequency noises. The $M \times 1$ coefficients vector of a Gaussian kernel $g[m]$ are computed as

$$g[m] = e^{-\frac{1}{2}\frac{(m-\frac{\mathrm{M}}{2})^2}{\sigma^2}} \qquad m = 1, 2, 3, ..., \mathrm{M} \qquad (1)$$

where M denotes the length of Gaussian kernel and σ denotes the width spread (or standard deviation) of the Gaussian kernel. The width of the Gaussian kernel is directly related to the value of σ. A larger value of σ produces a more larger pulse width. Then, Gaussian derivative kernel is computed as

$$h[m] = g[m+1] - g[m] \qquad m = 1, 2, 3, ..., \mathrm{M}-1 \quad (2)$$

The Gaussian kernel with pulse width of 100 ms and spread σ of 80 ms is used for noise suppression. The filtered signal $f[n]$ is obtained by taking the convolution of a signal $x[n]$ and Gaussian derivative kernel $h[n]$. The output of the filtering step is shown in Fig. 2(b) for the noisy PPG signal as shown

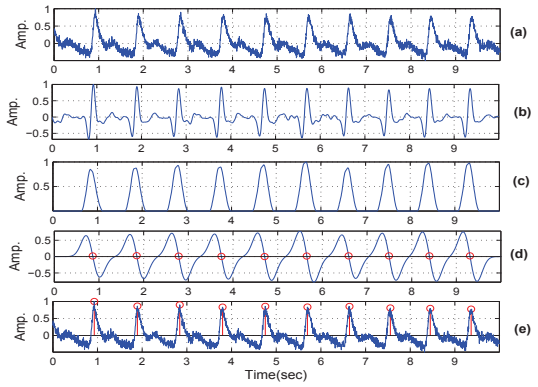

Fig. 2. Illustrates systolic peak detection performance for noisy PPG signal. (a) Original signal, (b) Output of the GDF stage, (c) Output of the Shannon energy envelope extraction stage, (d) Output of the GDF-based peak finding stage, and (e) systolic peak detection results.

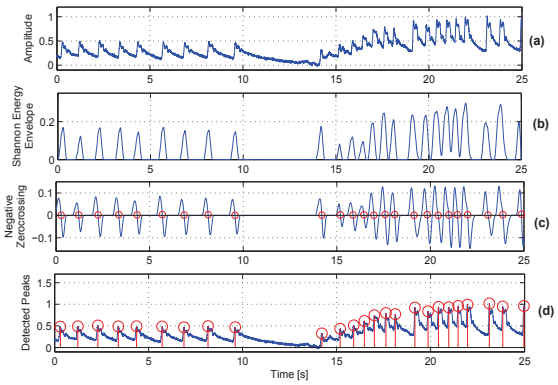

Fig. 3. Illustrates systolic peak detection performance for noisy PPG signal with different pulse morphologies. (a) Original signal, (b) Output of the Shannon energy envelope extraction stage, (c) Output of the GDF-based peak finding stage, and (d) systolic peak detection results.

in Fig.2(a). The results show that the GDF based filtering approach adequately suppresses the background noises and emphasizes the systolic portions.

B. Systolic Peak Detection

The systolic peak detection stage consists of three major steps: nonlinear peak amplification, Gaussian derivative based peak finding scheme, and peak position adjustment procedure.

1) Squaring and Adaptive thresholding: The filtered signal $f[n]$ is first squared to obtain a positive-valued signal and then adaptive thresholding is performed on the energy signal $e[n]$ that is computed as

$$e[n] = f^2[n]. \tag{3}$$

The squaring operation further suppresses the amplitudes of the low-frequency artifacts meanwhile it emphasizes the amplitude of the components of the systolic peaks. In order to remove the low-amplitudes of residual noise components the adaptive thresholding rule is implemented as

$$e_{th}[n] = \begin{cases} 0, & e[n] < \eta \\ e[n], & e[n] > \eta \end{cases} \tag{4}$$

where the threshold η is computed for each block. The adaptive threshold η for each PPG segment is computed as

$$\eta = \sqrt{\frac{1}{\mathrm{N}}\sum_{n=1}^{\mathrm{N}}(e[n]-\mu_e)^2} \text{ and } \mu_e = \frac{1}{\mathrm{N}}\sum_{n=1}^{\mathrm{N}} e[n].$$

where N is the number of samples.

2) Shannon Energy Envelope (SEE) Signal Extraction: Although the squaring operation suppresses the residual noise components, it also diminishes amplitude of low-amplitude pulsatile waveforms that may be buried in the high-amplitude pulsatile waveforms. Therefore, we employ Shannon energy operation that can significantly reduce the peak-amplitude deviations between smaller systolic peaks and high-amplitude peaks. The Shannon energy of the normalized signal is computed as

$$s[n] = -\tilde{e}_{th}^2[n]\log\tilde{e}_{th}^2[n]. \tag{5}$$

where $e_{th}[n]$ denotes the thresholded energy signal that is computed as

$$\tilde{e}_{th}[n] = \frac{e_{th}[n]}{\max_{n=1}^{\mathrm{N}}(|e_{th}[n]|)}. \tag{6}$$

The multiple peaks in the Shannon energy envelope (SEE) signal may increase number of false positive detections. Therefore, the envelope smoothing process is implemented using a linear zero-phase filtering with a rectangular impulse response, $h(k)$ of length L. The smoothing filter is designed to provide smoothed peaked-waves around systolic peak portions and to smooth out the multiple peaks. The smoothness depends on the filter length L, which is found empirically. In this work, window length of 150 ms is chosen that is less than refractory period of 300 ms. The output of the SEE extraction step is shown in Fig. 2(c). It can be observed that the time-instants of candidate systolic peaks in the smooth SEE signal $s[n]$ correspond to approximate time-instants of the systolic peaks in the PPG signal. Therefore, the candidate peaks are first detected and then used as guides to determine time-instants of true systolic peaks in the input PPG signal.

3) Peak Location Determination and Correction Rule: In this step, the time-instants of candidate systolic peaks are automatically determined by processing the negative zero-crossing points of the output waveform obtained from the convolution of the Shannon energy envelope signal $s[n]$ with Gaussian derivative kernel $d[n]$ with width (M) of 2 s and spread of $\sigma = 240$ ms. The convolution between these two signals is computed as

$$z[n] = \sum_{k=-\infty}^{\infty} d[k]\ s[n-k]. \tag{7}$$

The output of the convolution stage is shown in Fig. 2(d) for the envelope signal as shown in Fig. 2(c). It is observed from the Fig. 2(d) that the negative zerocrossing points correspond to the locations of the local peaks of the Shannon energy envelope $s[n]$ shown in Fig. 2(c). Therefore, the negative zero-crossing points are detected and used as guides to find

locations of true systolic peaks in the original PPG signal shown in Fig. 2(a). The output of the negative zerocrossing point determination step is shown in Fig. 2(d). The peak location adjustment procedure is employed to correct the errors of peak position shift due to the signal smoothing steps. In the correction procedure, a PPG segment centered around a detected location $(p[m] \pm \frac{w}{2})$ is extracted from the PPG signal and then location of maximum amplitude of the extracted PPG segment is computed to locate true systolic peaks in PPG signal. The window size (w) is set to 120 ms. The peak correction procedure is repeated for all the detected candidate locations $p[m]$. The final detected systolic peaks are marked in the PPG signal as shown in Fig. 2(e). The peak detection results shown in Figs. 2 and 3 demonstrate the effectiveness of the systolic peak detection approach under different types of pulsatile waveform morphologies and noise conditions.

TABLE I
ENSEMBLE AVERAGED PULSATILE WAVEFORM EXTRACTION ALGORITHM

Function: [b, eab]=EnsembleAveragedBeat
Initialization: L, nshift.
// L : Length of period normalized pulse and nshift : Shifting constant.
Inputs:
$s[n]$:= Input signal and $r[k]$:= Location vector of real peaks in PPG signal.
// K : Total number of systolic peaks and M : Length of subsegment.
Outputs: $b[t, l]$:= Peak aligned PPG beat sequences;
where t denotes number of beats.
$eh[l]$:= Ensemble averaged PPG beat sequence; $l = 1, 2, ..., \mathrm{L}$.
Beat Extraction, Peak Alignment and Averaging
for i= 1 to K-1;
Read PPGbeat: $s1[m] = s[r[i] : r[i+1]]$; $m = 1, 2, ..., \mathrm{M}$,
Left shifting: $s2[m] = s1[r[i] - \mathrm{nshift} : r[i+1] - \mathrm{nshift}]$,
Peak aligning by circular shifting: $s3[m] = \tilde{s2}[m - \mathrm{nshift} - 1]_{\mathrm{M}}$,
where $\tilde{s2}[m]_{\mathrm{M}}$ is considered as a circular sequence of length M,
Perform period normalization: $s4[l] = \mathrm{interpft}(s3, \mathrm{L})$,
Perform amplitude normalization: $s5[m] = s4[m]/|\max(s4[m])|$,
Perform peak centering: $s6[m] = \mathrm{fftshift}(s5[m])$,
Construct ECG beat matrix: **b[i,:]**:= $s6[m]$,
End.
Perform ensemble averaging: **eh[m]**:= $\frac{1}{P}\sum_{p=1}^{P}(b[p, :])$.

C. Ensemble Averaged Pulsatile Waveform Extraction

In this work, we obtain a PPG biometric identifier based on ensemble averaging of time-instant aligned segmented pulsatile waveforms of the PPG signal of an individual. In the enrollment phase, the pulsatile waveforms obtained for 20 s PPG signal are used to construct one ensemble averaged pulsatile waveform for each of the individuals in the enrollment phase. For P sets of pulsatile waveforms from the PPG signal of an each individual, the ensemble averaging process is implemented as

$$eh[k] = \frac{1}{P}\sum_{p=1}^{P} b_p[k], k = 1, 2, 3.....K \qquad (8)$$

b_p denotes the p^{th} pulsatile waveforms with length of K and eh denotes the ensemble pulsatile waveforms. Under the presence of the recording instrument noise (or random noise), the ensemble averaging can reduce the residual noise components in the pulsatile signal. The ensemble pulsatile waveforms obtained for all of individuals are stored in the enrollment database. The ensemble averaged pulsatile waveform extraction stage includes the steps of: pulsatile waveform segmentation, period and amplitude normalization, S-peak alignment and ensemble averaged pulsatile waveform computation. The algorithm for the extraction of ensemble averaged pulsatile waveform is illustrated in Table I.

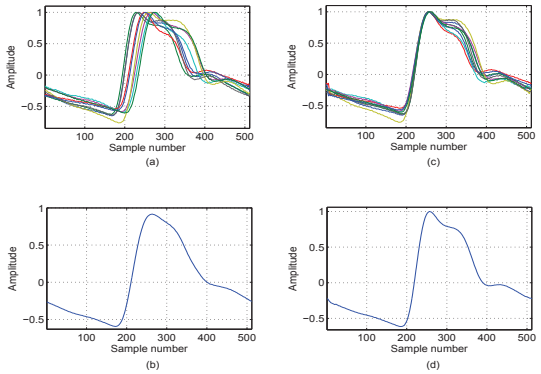

Fig. 4. Illustrates the effectiveness of the ensemble averaged pulsatile waveform extraction stage using Systolic peak (S-peak) alignment. (a) pulsatile waveforms without S-peak alignment, (b) ensemble averaged pulsatile waveform without S-peak alignment, (c) pulsatile waveforms with S-peak alignment, (d) ensemble averaged pulsatile waveform with S-peak alignment.

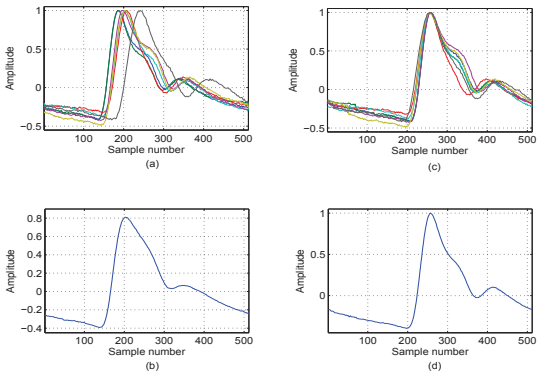

Fig. 5. Illustrates the effectiveness of the ensemble averaged pulsatile waveform extraction stage using S-peak alignment. (a) pulsatile waveforms without S-peak alignment, (b) ensemble averaged pulsatile waveform without S-peak alignment, (c) pulsatile waveforms with S-peak alignment, (d) ensemble averaged pulsatile waveform with S-peak alignment.

The outputs of the ensemble averaged pulsatile waveform extraction algorithm are illustrated in Figs. 4-5 for PPG signals with different pulsatile morphologies. From the results as shown in Fig. 4(a) and (b) and Fig. 5(a) and (b), we can observe that the local features of the original pulsatile waveforms are not preserved in the constructed ensemble averaged pulsatile waveform without using the Systolic peak (S-peak) alignment process. The extracted ensemble averaged pulsatile waveforms using the S-peak alignment process are shown in Fig. 4(d) and Fig. 5(d). It can be observed that the morphological features of the original pulsatile waveforms

are significantly preserved in the extracted ensemble averaged pulsatile waveform.

D. Similarity Metrics For Template Matching

In this subsection, we study the effectiveness of the different similarity metrics (including, normalized cross correlation (NCC) [17], [18], [19], wavelet weighted-based PRD (WWPRD) [18] and wavelet distance measure (WDIST) [19], [20]) that are used in the existing biometric authentication methods. For the test pulsatile waveform template x_t, and the enrolled pulsatile waveform template x_{e_i} for subject $i(i = 1, 2, ..., M; M$ is the number of subject enrolled in the biometric database), the NCC is computed as [17], [18], [19]

$$\mathrm{NCC}_i = \frac{\sum_{n=1}^{N}(x_t(n) - \bar{x}_t)(x_{e_i}(n) - \bar{x}_{e_i})}{\sqrt{\sum_{l=1}^{N}(x_t(l) - \bar{x}_t)^2 \sum_{k=1}^{N}(x_{e_i}(k) - \bar{x}_{e_i})^2}} \tag{9}$$

where $\bar{x}_t$ denotes the mean of test template x_t, and $\bar{x}_{e_i}$ denotes the mean of enrolled template x_{r_i} for subject *i*. The wavelet distance (WDIST) is computed as [19], [20]

$$\mathrm{WDIST}_i = \sum_{p=1}^{P}\sum_{q=1}^{Q} \frac{|\gamma_t^{p,q} - \gamma_{r_i}^{p,q}|}{max(|\gamma_t^{p,q}|, \tau)} \tag{10}$$

where $\gamma_t^{p,q}$, $\gamma_{r_i}^{p,q}$ denote detail coefficients of the discrete wavelet transforms ($\gamma^{p,q}$; detail coefficient q from the pth level of decomposition) of unknown signal and enrolled data for subject *i* respectively. The denominator is used to weigh the contribution of the absolute difference $|\gamma_t^{p,q} - \gamma_{r_i}^{p,q}|$ based upon the relative amplitude of the wavelet coefficient from the unknown signal. The threshold value τ is used to avoid relatively small wavelet coefficients from overemphasizing differences. The WWPRD is computed as [18]

$$\mathrm{WWPRD} = \sum_{l=1}^{\mathrm{L}+1} w_l \mathrm{WPRD}_l \times 100 \tag{11}$$

where,

$$w_l = \frac{\sum_{k=1}^{\mathrm{K}_l} d_l[k]}{\sum_{m=1}^{\mathrm{L}+1}\sum_{k=1}^{\mathrm{K}_l} d_m[k]};\ l = 1, 2, ..., (\mathrm{L}+1). \tag{12}$$

d_1-d_{L} are detail coefficients and $d_{\mathrm{L}+1}$ is approximation coefficient of wavelet decomposition of level-L, K_l denotes the number of coefficients in d_l and

$$\mathrm{WPRD}_l = \sqrt{\frac{\sum_{k=1}^{\mathrm{K}_l}(d_l[k] - \tilde{d}_l[k])^2}{\sum_{k=1}^{\mathrm{K}_l}(d_l[k])^2}} \tag{13}$$

In the next Section, we present the effectiveness of the above mentioned similarity metrics under different noise conditions.

III. Results and Discussion

We study the performance of the PPG-based biometric methods that have been developed using the proposed ensemble averaged pulsatile waveform extraction approach and three similarity measures such as NCC [19], [18], [17], WDIST [19], [20] and WWPRD [18]. In this work, the PPG signals are collected from the standard pulse signal databases: MIT-BIH Polysomnographic Database (slpdb) and Challenge 2014 Training Set (Challenge/2014/set-p). The pulse signals are sampled at rate of 250 Hz. The three PPG biometric methods are tested and validated using 24 genuine and 6 imposter subjects with total of 30 subjects. In the training phase, the ensemble averaged pulsatile waveform is constructed from pulse signal duration of 20 s for each of the subjects. The total number of enrolled subjects is 24. In the testing phase, we created 567 test segments for each of the genuine and imposter subjects. Each segment duration is 10 s. The total numbers of test segments for the genuine and imposter subjects are 13608 and 3402, respectively. In this study, the authentication is performed based on the pulsatile beat-by-beat correlation analysis of 10 s pulse signal from each subject. The rejection or acceptance of subject is performed based on the maximum similarity score which is greater than the half of the total number of beats of the 10 s pulse signal. The similarity score is computed based on the binary matching scores obtained for the optimal correlation threshold.

For validation purposes, we compute the three benchmark parameters [5]: false acceptance rate (FAR), false rejection rate (FRR) and equal error rate (EER) that are defined as

$$\mathrm{FAR} = \frac{\mathrm{FA}}{\mathrm{NI}} \quad \text{and} \quad \mathrm{FRR} = \frac{\mathrm{FR}}{\mathrm{NG}} \tag{14}$$

where FA denotes number of false acceptances by the system, NI denotes the number of impostors, FR denotes number of false rejections and NG denotes number of genuine subjects. The equal error rate (EER) is defined as the rate at which the false acceptance rate equals the false rejection rate [5]. The value of the EER can be easily obtained from the receiver operating characteristics (ROC) curve that ranges between 0 and 1. The ROC curves for three authentication methods are shown in Fig. 6. From the ROC curve of each of the biometric methods, the optimal threshold is found for further testing and validation of the three biometric methods under different noise conditions and noise levels.

From the results as shown in Fig. 6, the optimal threshold for the NCC-based method is 0.997 whereas the optimal thresholds for the WWPRD- and WDIST-based methods are 12.8 and 6.3, respectively. The EER values are 0.29, 0.325, and 0.45, respectively. For the optimal thresholds, we study the robustness of the three biometric methods under different SNR values and noise types. The experimental results of this study are summarized in Table II. The authentication results show that the PPG biometric method using the NCC metric yields better performance with FAR of 0.24 and FRR of 0.41 for SNR value of 20 dB. Moreover, the NCC based method demonstrates the better authentication results for clean

TABLE II

PERFORMANCE COMPARISONS OF PPG BASED BIOMETRIC AUTHENTICATION METHODS USING DIFFERENT TEMPLATE MATCHING MEASURES.

Methods	η_{opt}	Clean		AWGN, Signal-to-Noise Ratio (SNR)												BW		PLI	
				40 dB		35 dB		30 dB		25 dB		20 dB		15 dB					
		FAR	FRR	FAR	FRR	FAR	FRR	FAR	FRR	FAR	FRR	FAR	FRR	FAR	FRR	FAR	FRR	FAR	FRR
NCC	0.997	0.32	0.32	0.33	0.33	0.31	0.33	0.33	0.34	0.28	0.31	0.24	0.41	0.15	0.65	0.34	0.34	0.32	0.32
WWPRD	12.8	0.34	0.34	0.32	0.34	0.33	0.33	0.33	0.35	0.26	0.41	0.12	0.56	0.05	0.85	0.28	0.37	0.34	0.34
WDIST	6.3	0.46	0.46	0.39	0.45	0.33	0.50	0.18	0.58	0.09	0.81	0.02	0.98	0.000	1.000	0.32	0.53	0.46	0.46

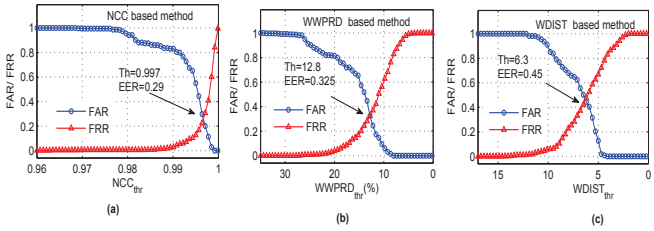

Fig. 6. Illustrates the FAR and FRR for different thresholds of three PPG-biometric methods. (a) NCC based method, (b) WWPRD-based method, and (c) WDIST-based method. The equal error rate (EERs) at their optimal thresholds are marked.

and noisy PPG signals. From the authentication results, it is observed that the Gaussian derivative based filtering approach can provide better detection rates in case of PPG signals with baseline wanders and powerline interference. Unlike the existing methods using DWT, EMD and PCA/ICA, and adaptive filters, the proposed systolic peak detection approach uses simple filtering technique. From our experimental results, it is noted that the proposed approach yields detection accuracy of 99.5-100% for most PPG signals including different pulse morphologies, baseline wanders, and powerline interference. The PPG biometric method using ensemble averaged pulsatile waveform and NCC metric achieves a FAR of 0.32 and FRR of 0.32 for the threshold of 0.997. The proposed method outperforms the other wavelet distance based methods. By comparing the complexity of the functional blocks of existing methods, we believe that the PPG biometric method based on the pulsatile waveform correlation is simple compared to the local features and machine learning based PCG biometric methods. In the future directions, we study effectiveness of the PPG biometric under different physical activities.

IV. CONCLUSION

In this paper, we present PPG biometric method using pulsatile waveform correlation. The proposed method consists of four stages: preprocessing, systolic peak detection, ensemble averaged pulsatile waveform extraction, and similarity matching. The proposed method is tested and validated using the PPG signals taken from 24 genuine and 6 imposter subjects. Performance evaluation results show that the PPG biometric method using NCC metric achieves a FAR of 0.32 and FRR of 0.32 for the threshold of 0.997 that outperforms the other wavelet distance based methods which have higher computational load. Results show that the proposed method has great potential in wireless body area networks and m-health applications.

REFERENCES

[1] C. Chen *et al.*, "A chaotic theoretical approach to ECG-based identity recognition," *IEEE Comput. Intell. Mag.*, vol. 9, no. 1, pp. 53-63, 2014.

[2] M. D. Bugdol and A.W. Mitas, "Multimodal biometric system combining ECG and sound signals," *Pattern Recog. Lett.*, vol. 38, pp. 107-112, 2014.

[3] J. Wang, M. She, S. Nahavandi, and A. Kouzani, "Human identification from ECG signals via sparse representation of local segments," *IEEE Signal Process. Lett.*, vol. 20, no. 10, pp. 937-940, 2013.

[4] Z. Zhang, H. Wang, A. V. Vasilakos, and H. Fang, "ECG-Cryptography and authentication in body area networks," *IEEE Trans. Inf. Technol. Biomed.,* vol. 16, no. 6, pp. 1070-1078, Nov. 2012.

[5] M. A.-Zahhad, S. M. Ahmed, and S. N. Abbas, "Biometric authentication based on PCG and ECG signals: present status and future directions," in *Signal, Image and Video Processing*, vol. 8, no. 4, pp. 739-751, 2014.

[6] A. Bonissi *et al.*, "A preliminary study on continuous authentication methods for photoplethysmographic biometrics," in *Proc. IEEE Workshop on Biometric Measurements and Systems for Security and Medical Applications (BioMS)*, pp. 28-33, 2013.

[7] N. S. G. R. Salanke, A. Samraj, N. Maheswari, and S. Sadhasivam, "Enhancement in the design of biometric identification system based on photoplethysmography data," in *Proc. IEEE Int. Conf. Green High Performance Computing (ICGHPC)*, pp. 1-6, 2013.

[8] P. Spachos, J. Gao, and D. Hatzinakos, "Feasibility study of photoplethysmographic signals for biometric identification," in *Proc. IEEE Int. Conf. Digital Signal Processing (DSP)*, pp. 1-5, 2011.

[9] J. Yao, X. Sun, and Y. Wan, "A pilot study on using derivatives of photoplethysmographic signals as a biometric identifier," in *Proc. IEEE Conf. Eng. Med. and Bio.* , 2007.

[10] S.-D. Bao, Y.-T. Zhang, and L.-F. Shen, "Physiological signal based entity authentication for body area sensor networks and mobile healthcare systems," in *Proc. IEEE Conf. Eng. Med. Bio.*, pp. 2455-2458, 2005.

[11] Y. Y. Gu, Y. Zhang, and Y. T. Zhang, "A novel biometric approach in human verification by photoplethysmographic signals," in *Proc. IEEE Conf. Inf. Tech. Appl. Biomed.*, pp. 13-14, 2003.

[12] Y. Y. Gu and Y. T. Zhay, "Photoplethysmographic authentication through fuzzy logic," in *Proc. IEEE EMBS Conf. Biomedical Engineering*, pp. 136-137, 2003.

[13] N. S. G. R. Salanke, N. Maheswari, and A. Samraj, "An enhanced intrinsic biometric in identifying people by photopleythsmography signal," in *Proc. Int. Conf. Signal and Image Proces. (ICSIP)*, pp. 291-299, 2012.

[14] A. D. O.-Canon *et al.*, "Onset and peak pattern recognition on photoplethysmographic signals using neural networks," *Progress in Pattern Recognition, Image Analysis, Computer Vision, and Appl.*, pp. 543-550, 2013.

[15] A. R. Kavsaoglu, K. Polat, and M. R. Bozkurt, "A novel feature ranking algorithm for biometric recognition with PPG signals," *Computers in Biology and Medicine*, vol. 49, pp. 1-14, 2014.

[16] M. M. Tantawi, K. Revett, A.-B. Salem, and M. F. Tolba, "A wavelet feature extraction method for electrocardiogram (ECG)-based biometric recognition," *Signal, Image and Video Processing*, pp. 1-10, 2013.

[17] C. Hegde *et al.*, "Heartbeat biometrics for human authentication," *Signal, Image and Video Processing*, vol. 5, no. 4, pp. 485-493, 2011.

[18] A. S. Al-Fahoum, "Quality assessment of ECG compression techniques using a wavelet-based diagnostic measure," *IEEE Trans. Inf. Technol. Biomed.,* vol. 10, no. 1, pp. 182?191, Jan. 2006.

[19] A. D. C. Chan, M. M. Hamdy, A. Badre, and V. Badee, "Wavelet distance measure for person identification using electrocardiograms," *IEEE Trans. Instrum. Meas.,* vol. 57, no. 2, pp. 248-253, Feb. 2008.

[20] K. A. Sidek and I. Khalil, "Enhancement of low sampling frequency recordings for ECG biometric matching using interpolation," *Computer Methods and Programs in Biomedicine,* vol. 109, no. 1, pp. 13-25, 2013.